Geospatial assessment of above-ground biomass degradation in forest habitats of the "Svyati Hory" National Nature Park due to armed conflict-related wildfires (2022–2024)

Oleksandr Harbar[1,*], Olha Chusova[2], Polina Hetman[2], Yakiv Didukh[2]

[1] Zhytomyr Ivan Franko State University, Department of Ecology and Geography, Ukraine
[2] M. G. Kholodny Institute of Botany, Department of Geobotany and Ecology, Ukraine
[*] Corresponding author: o.v.harbar@gmail.com

ABSTRACT

This study develops a method for assessing above-ground biomass (AGB) in forest habitats of the "Svyati Hory" National Nature Park and quantifies its degradation caused by armed conflict-related wildfires in 2022–2024. A multisensor approach integrating Sentinel-1 and Sentinel-2 data, the Copernicus GLO-30 DEM and GEDI LiDAR measurements was applied via a Random Forest regression model calibrated with forest inventory records. Comparative analysis confirmed the superiority of the 10 m spatial scale ($R^2 = 0.575$) over 20 m and 30 m resolutions for fragmented mosaic landscapes. The model demonstrated strong predictive performance (RMSE 15.3–17.7 Mg/ha), enabling rapid biomass updates when field surveys are hindered by limited accessibility to the area. Results indicate that the park's total baseline AGB was 14.22 million tonnes across 37.1 thousand hectares. Burn scar mapping and spatial overlay analysis revealed a total loss of 4.66 million tonnes of biomass over 11.96 thousand hectares. The highest losses occurred in Sarmatic steppe pine forests, which lost 68.2% of their biomass. The relict chalk pine forests (Pinus sylvestris var. cretacea) were likewise severely affected, losing 36.6% of their area, thereby threatening the natural regeneration of this endemic population.

KEYWORDS

above-ground biomass; remote sensing; forest fires; environmental damage; military operations

Received: 7 July 2026
Accepted: 12 October 2026
Published online: 3 November 2026

Harbar, O., Chusova, O., Hetman, P., Didukh, Y. (2026): Geospatial assessment of above-ground biomass degradation in forest habitats of the "Svyati Hory" National Nature Park due to armed conflict-related wildfires (2022–2024). AUC Geographica, e23361980.2026.17
https://doi.org/10.14712/23361980.2026.17
© 2026 The Authors. This is an open-access article distributed under the terms of the Creative Commons Attribution License (https://creativecommons.org/licenses/by/4.0).

1. Introduction

The armed conflict causes substantial damage to the environment by disrupting and destroying ecosystem structures. Forest ecosystems are severely affected by the conflict-related fires, including those ignited by shelling and munitions strikes, particularly when active hostilities prevent timely fire suppression. (Matsala et al. 2024; Pereira et al. 2022; Zibtsev et al. 2024). Ukraine has experienced a marked increase in wildfire frequency and burned areas, significantly exceeding the European average. According to the European Commission's Joint Research Centre, the forest area affected by wildfires in Ukraine in 2024 was twice that recorded across the entire European Union (Sedano et al. 2026). Protected forests hold exceptional ecological value, but they are were not spared from destruction:in the "Svyati Hory" National Nature Park, wildfires destroyed 11.96 thousand hectares of forest land, accounting for 28.7% of its total area. Consequently, this park was selected for remote-sensing-based estimation of biomass losses. This approach enables the refinement of environmental damage assessment frameworks, providing critical documentation required by legal authorities for reparations.

Satellite remote sensing enables high-resolution monitoring of above-ground biomass (AGB) and its dynamics across large areas (Harris et al. 2021). Although biomass estimation depends on sound allometric models and robust field measurements, the traditional data gathering is highly labor-intensive and time-consuming, which is prompting a shift toward remote sensing. Modern land monitoring increasingly relies on integrated open-access datasets, including Sentinel-1 (S1) radar imagery, Sentinel-2 (S2) multispectral optical data, and spaceborne LiDAR from the GEDI (Global Ecosystem Dynamics Investigation) mission (Shao and Zhang 2016).

Operating since April 2019 aboard the International Space Station, GEDI is the first satellite LiDAR mission designed to study the vertical structure of vegetation, measuring canopy profile characteristics at a 25 m spatial resolution between latitudes 51.6°N and 51.6°S (Dubayah et al. 2022). Integrating multiple spaceborne sensors represents the

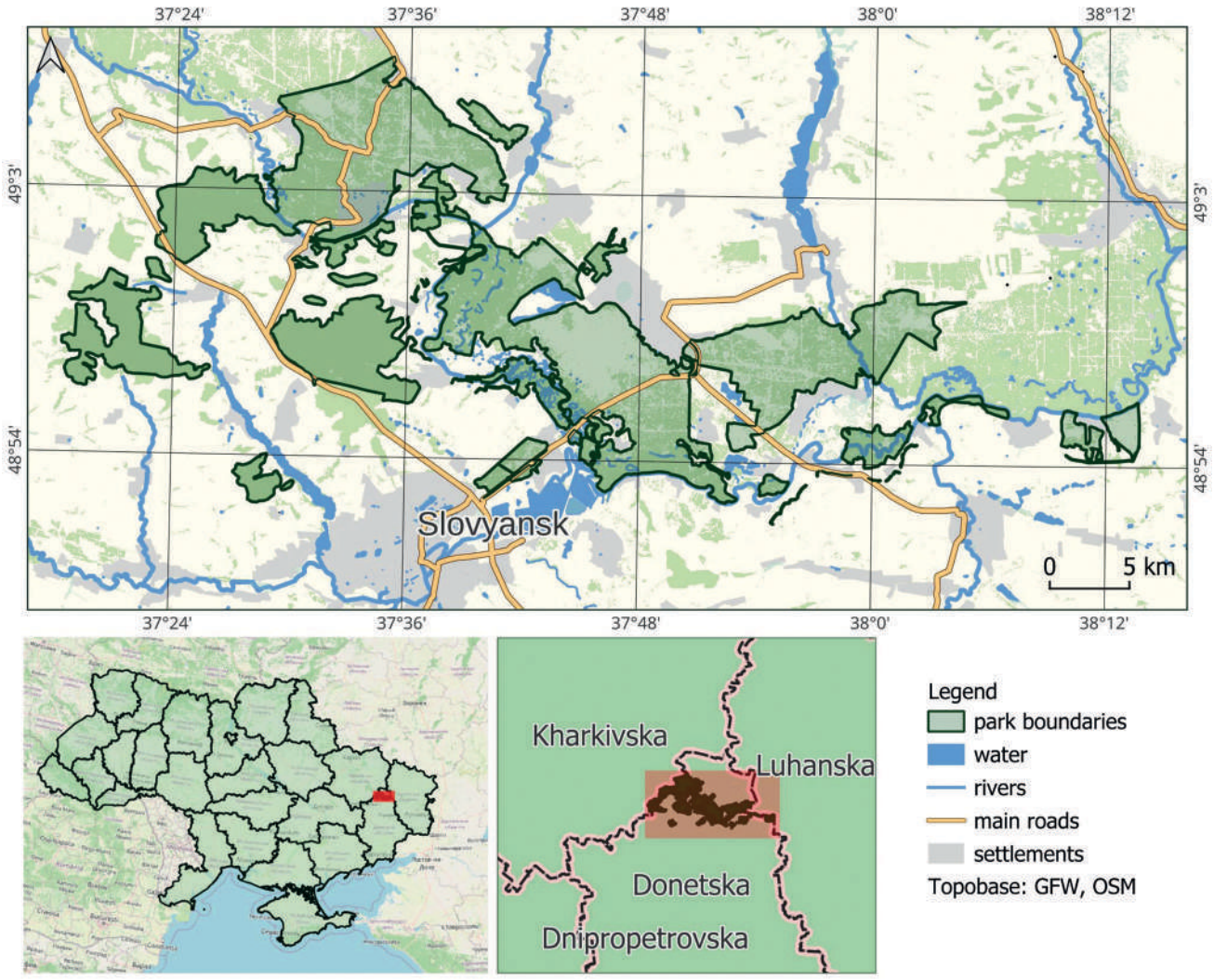


Fig. 1 Geographical location and boundaries of the "Svyati Hory" National Nature Park.

most effective approach for biomass mapping. For instance, GEDI-derived canopy parameters have been combined with Landsat imagery to develop global forest height models at 30 m resolution (Potapov et al. 2021), and with Sentinel-2 data to generate 10 m resolution global maps (Lang et al. 2023). Similar multisensor integration involving S1, S2, and GEDI metrics has been successfully applied to regional canopy height and biomass modeling (Fayad et al. 2024; Pauls et al. 2024; Tolan et al. 2024).

Given the worsening climate crisis, accurate forest carbon management and vertical structure assessments are vital. GEDI data have proven highly effective for evaluating AGB density and carbon stocks in protected areas and managed forests globally, as demonstrated in recent studies across various geographic scales (Liang et al. 2023; Grings et al. 2025; Van Winckel et al. 2025).

Building upon these findings, this study aims to evaluate the above-ground phytomass of the "Svyati Hory" National Nature Park by modeling AGB density (AGBD) using the Random Forest machine learning algorithm integrated with multispectral satellite data (Sentinel-2), radar data (Sentinel-1), terrain parameters derived from the Copernicus GLO-30 DEM and GEDI LiDAR measurements. Furthermore, we aim to verify these modeling outputs against historical forest inventory data and quantify the total forest stock losses resulting from wildfires caused by the armed conflict.

2. Materials and methods

2.1 Study area

The "Svyati Hory" National Nature Park (Fig. 1), established in 1997 in the Bakhmut and Kramatorsk districts of the Donetsk region, serves as the study area. Spanning the high right bank, the lower pine terrace, and the Siverskyi Donets River floodplain, the park covers 40.6 thousand hectares, with forests occupying 95% of the territory. The average age of these forest stands is 73 years, with a mean canopy height of 19.67 m, an average DBH of 25.03 cm, and a growing stock volume of 212.33 m^3/ha. Relict chalk pine forests (*Pinus sylvestris* on chalk) hold high ecological value (Kotov 1928); in the 1960s–1970s, they extended over 90 hectares, forming the largest contiguous tract within the Serednyoruska Upland (Doronin 1970). Additionally, the left bank contains artificial pine plantations established in the 1950s–1960s adjacent to natural peri-steppe pine forest remnants exceeding 140 years of age. The area also hosts upland, ravine, and floodplain oak forests, alder groves, and poplar-willow forests (Didukh and Pashkevych 2003).

In the Mayatska Dacha tract, an isolated locality of *Carpinus betulus* L. occurs (Sinelshchikov 1975). Detailed vegetation characteristics of these habitats, which have recently suffered severe degradation and loss, are provided in subsequent studies (Dyakova 2008; Zhurova 2012; Kuzemko et al. 2018; Didukh et al. 2024).

2.2 Methodology for Modelling Aboveground Biomass Density (AGBD)

Aboveground biomass density (AGBD) was modeled via Google Earth Engine (Gorelick et al. 2017) using a machine learning approach based on optical and radar satellite data calibrated against GEDI LiDAR measurements. The target variable was derived from the GEDI L4A AGBD product, which provides high-precision footprints for model training. To effectively capture canopy structure, moisture status, and terrain influences, the predictor stack incorporated multi-source remote sensing metrics: Sentinel-2 optical bands (B1–B8, B8A, B9, B11, B12) and derived spectral indices (NDVI, EVI, NDRE) to account for vegetation greenness, chlorophyll content, and canopy closure; Sentinel-1 radar backscatter (VV and VH polarizations) to mitigate spectral saturation and capture structural forest density; and Copernicus GLO-30 DEM parameters (elevation and slope) to account for geomorphological controls on biomass distribution.To minimize systematic errors, GEDI data underwent multicriteria filtering, retaining points with l4_quality _flag = 1, degrade_flag = 0, relative biomass estimation error ≤ 50%, and terrain slopes ≤ 30%. Water bodies (NDWI < 0.1) and non-forest areas (Landsat tree cover ≤ 15%) were masked out. All datasets were harmonized to a 10-meter spatial resolution (EPSG:3857) using bilinear interpolation and the reduceResolution method.

Regression was performed using the Random Forest algorithm (smileRandomForest) with 500 decision trees, trained on a stratified sample of 4,000 points (70% training, 30% validation). Model accuracy was evaluated using the Root-Mean-Square Error (RMSE, Mg/ha), relative RMSE (RMSE%), and Coefficient of Determination (R^2). Predictor relative importance (%) was also calculated to identify the primary drivers of biomass estimation.

2.3 Forest habitat mapping methodology

Forest habitats were mapped using a modified methodology based on the National Habitat Catalogue of Ukraine (Kuzemko et al. 2018). Habitats were identified according to the EUNIS classification system (EUNIS).

2.4 Methodology for quantifying forest stand areas destroyed by wildfires

The general workflow for processing Sentinel-2 imagery consisted of four stages implemented in three Google Earth Engine (GEE) scripts (Gorelick

et al. 2017): initial dataset creation, land-cover classification, classification accuracy assessment, and land-cover change detection. The classification procedure was based on an object-oriented approach using the Random Forest (RF) classifier (Tassi and Vizzari 2020). Classification accuracy was assessed using an error matrix based on validation datasets (Al-Saady et al. 2015).

2.5 Methodology for analysis and calibration of verification data

To estimate phytomass stocks, 2014 forest inventory data (sub-compartment area, height, DBH, age, stand density, and growing stock volume) were analyzed. To determine 2022 stock volumes, relationships between age, height, and diameter for dominant tree species were projected to 2022 using quadratic equations, applying linear models only to immature stands. Mean growing stock volume (m^3/ha) was calculated from age-volume, height-volume, and diameter-volume functions.

Dry wood biomass was determined using conversion factors from Groshev et al. (1980): 0.4 for coniferous; 0.55 for *Quercus robur*, *Tilia cordata*, *Fraxinus excelsior*, and *Acer negundo*; 0.45 for small-leaved deciduous; and 0.6 for *Robinia pseudoacacia*. Biomass of individual ecosystem components (stem wood, branches, foliage) was calculated using allometric ratios (Hylyarov 1967; Lakida 2002) and supplemented with shrub and herb layer indices. Young stands (< 20 years old) were excluded due to high heterogeneity. This approach compensated for the lack of 2022 inventory data.

Also for cross-validation, modeled above-ground biomass (AGB, Mg/ha) was compared with state forest management datasets of stem wood volume (V, m^3/ha) for 2014. AGB was calculated via the biomass expansion factor (BEF) method: AGB = V * K, where K is the integral conversion factor accounting for wood basic density and the mass of the components.

Differentiated K-coefficients were applied following Lakida (2002): coniferous (0.52), hard-leaved deciduous (0.60), and soft-leaved deciduous (0.59). To mitigate the inventory time gap and remove statistical outliers (e.g., undocumented logging), a two-stage hybrid filtering was applied. Outliers were removed using the Interquartile Range (IQR) method applied to model residuals, followed by filtering out observations exceeding the Mean Absolute Error (MAE) threshold.

To test for non-linearity between remote sensing and ground-truth data, linear and quadratic regression models were compared using the Coefficient of Determination (R^2) and Akaike's Information Criterion (AIC) at a significance level of $\alpha = 0.05$. Statistical analysis and visualization were performed using Python (v.3.x), and spatial analysis via QGIS 3.34.15.

Tab. 1. Quality estimates of aboveground biomass models for the "Svyati Hory" National Nature Park with different spatial resolutions.

Resolution	R^2 (coef. of determination)	RMSE (Mg/ha)	RMSE (%)
10 m	0.575	42.82	24.24
20 m	0.528	43.76	24.68
30 m	0.281	48.31	26.48

3. Results

3.1 Comparing the accuracy of models with different spatial resolutions

Different spatial resolutions (10 m, 20 m, and 30 m) are essential for understanding how scale affects the accuracy of biomass estimation (Tab. 1, Fig. 2).

A spatial resolution of 30 m (R^2 = 0.281) is characterized by the lowest accuracy (Tab. 1, Fig. 2 and Fig. 3). With a spatial resolution of 20 m (R^2 = 0.528), a noticeable increase in accuracy is observed as the resolution approaches that of the Sentinel-2 bands (Tab. 1, Fig. 2 and Fig. 3). However, local biomass peaks reflected in the overall correlation are still smoothed out.

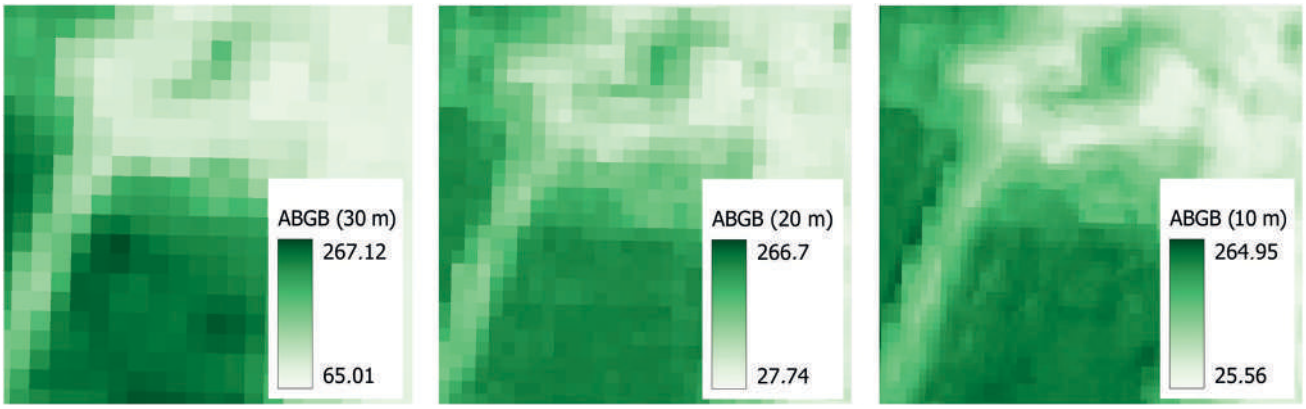


Fig. 2 Fragments of aboveground biomass maps (Mg/ha) near the Sosnove urban-type settlement at different spatial resolutions.

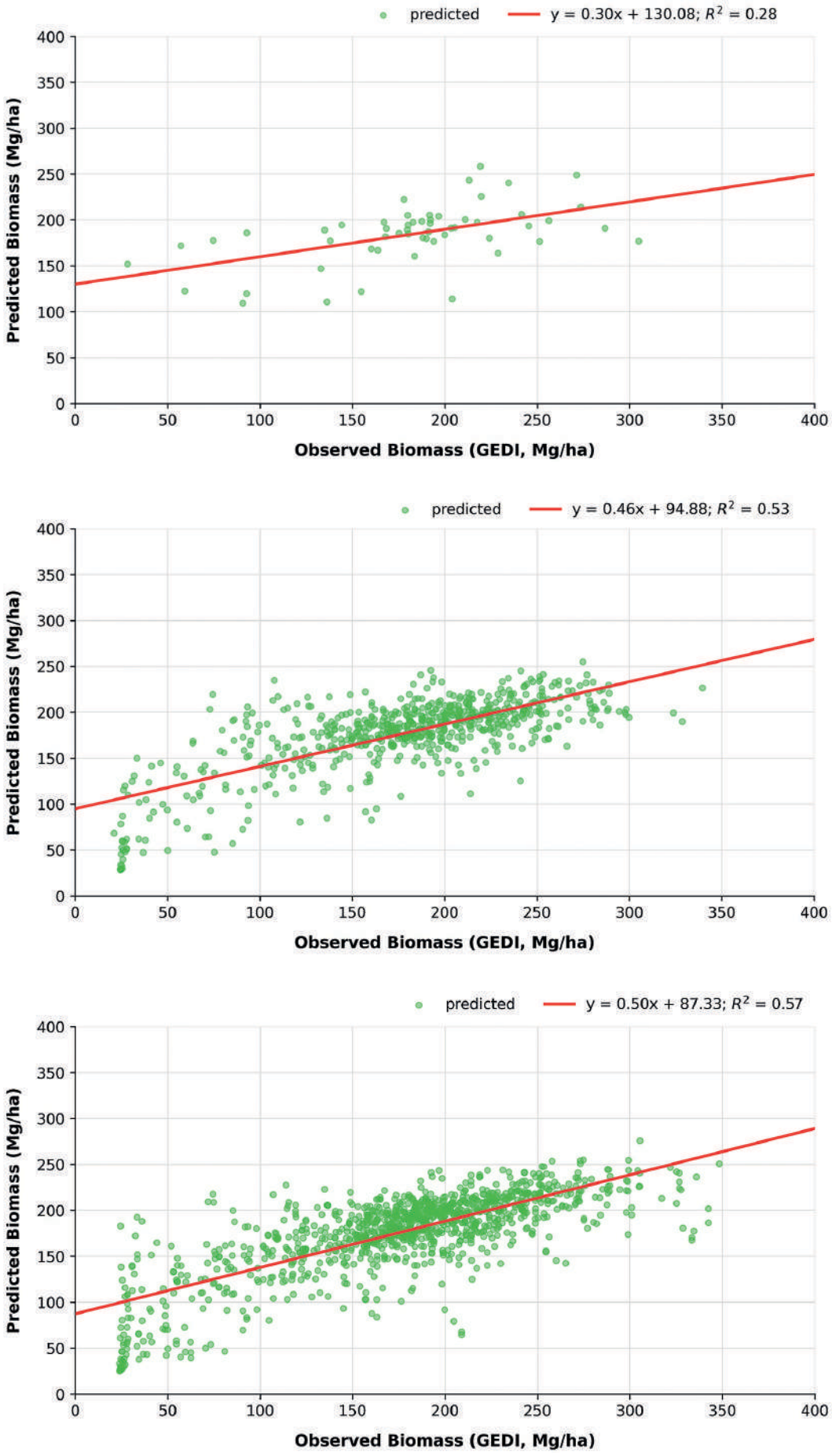


Fig. 3 Validation results of the model with a resolution of 30 m (a), 20 m (b), and 10 m (c).

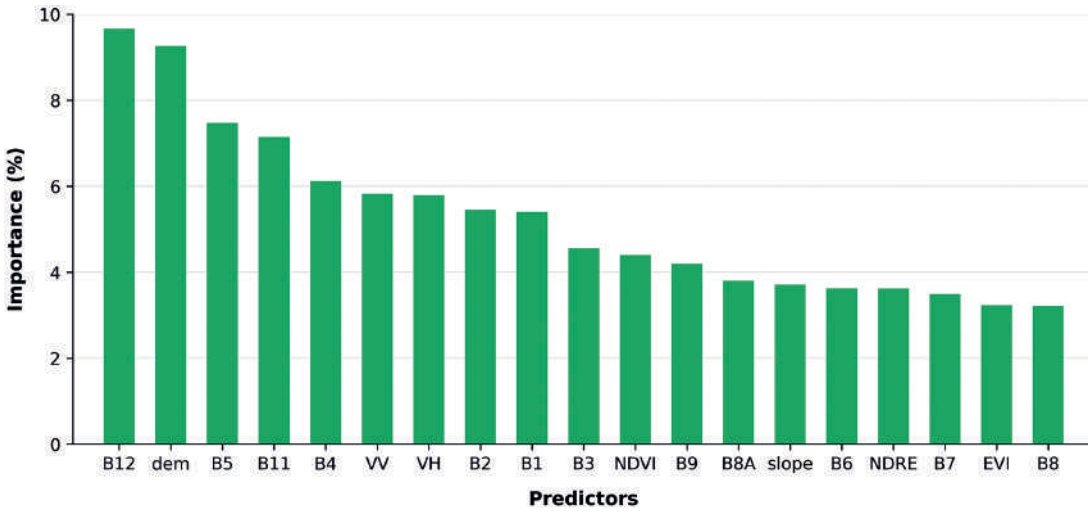


Fig. 4 Predictor importance estimates (%) for the 10-meter resolution aboveground biomass model (for acronym definitions, see the "Predictor Importance" section).

A spatial resolution of 10 m (R^2 = 0.575) delivers the best result among the three options (Tab. 1, Fig. 2 and Fig. 3). Higher resolution allows the model to capture spectral differences between tree canopies and reduces the number of "mixed" pixels at the boundaries of forest stands. The model explains 57.5% of the biomass variation. This is a high value for forest ecosystems, considering their complex structure. An error rate of 24.2% is entirely acceptable for remote sensing methods (up to 30% is generally considered the norm).

The most notable change during the transition from 30 m to 20 m and 10 m (Fig. 2) was a sharp transformation of the lower limit of biomass values in the legend. While the minimum value on the 30-meter map was 65.01 Mg/ha, it decreased to 25.56 Mg/ha on the 10-meter map. On maps with spatial resolutions of 20 m and 10 m, small infrastructure elements such as forest clearings and roads (light lines) are clearly visible, whereas on the 30-meter map, they appear blurred or intermittent. This is important for mapping areas bordering clearcuts or roads. Furthermore, the 10-meter map allows for the visualization of internal forest heterogeneity – "gaps" in stands and the microstructure of the canopy space. On coarser maps, these details are lost, turning the forest into a spectrally homogeneous expanse.

3.2 Predictor importance

Spectral bands and elevation exert the greatest influence on the model (Fig. 4). B12 (Short-wave Infrared – SWIR) provides the highest contribution (~9.7%), the Digital Elevation Model (DEM) ranks second (~9.3%), B5 (Red Edge) and B11 (SWIR) also exhibit high significance (~7.5% and 7.2%, respectively), vegetation indices (NDVI, EVI, NDRE) show moderate importance (ranging from 3.5% to 4.5%), radar data (VH, VV) maintain a stable, moderate influence (~5.8%), B8 (Near-Infrared) and B9 (Water Vapour) show the lowest values (~3.2%) and Slope has a relatively low impact (~3.8%).

Consequently, the model relies heavily on the short-wave infrared spectrum (SWIR) and topographical characteristics (DEM). This demonstrates that the "greenness" of plants (provided by the visible spectrum) is insufficient for accurate biomass prediction; it is essential to account for stand structure and environmental conditions.

Tab. 2 Forest inventory parameters of different tree species for 2014 and 2022.

Species	Area (ha)	Age		Height (m)		Diameter (cm)		Growing stock volume (m^3)	
		2014	2022	2014	2022	2014	2022	2014	2022
Quercus robur	5532.20	78.74±31.35	90.39±27.99	19.03±4.75	20.74±3.12	26.61±10.79	29.55±15.73	176.14±67.35	222.40±40.53
Pinus sylvestris	3339.99	43.49±18.63	49.49±18.6	13.22±5.38	14.45±2.66	17.37±7.67	25.31±8.85	236.17±90.73	268.03±40.12
Fraxinus excelsior	1056.91	67.59±25.13	73.59±25.13	20.78±4.87	22.04±3.45	25.19±8.32	29.00±8.64	199.32±73.31	215.02±39.01
Alnus glutinosa	398.40	55.70±22.49	61.69±22.49	18.85±6.03	20.53±4.45	21.50±7.45	25.88±4.86	190.96±87.34	219.25±54.82

3.3 Model validation based on data calculated for 2022 using forest management materials 2014

To validate the aboveground biomass model we used calculated data on biomass stocks within the forest compartments of the "Svyati Hory" National Nature Park, derived from forest management records (Tab. 2).

For further data verification analysis, we selected the parameters of four tree species: *Pinus sylvestris* s.l., *Quercus robur*, *Fraxinus excelsior*, and *Alnus glutinosa*. These species cover the largest areas (accounting for 96.7% of the total forested area) and represent diverse growing conditions ranging from dry to wet forest sites (Tab. 2).

As illustrated by the age-dependent changes in the growing stock volume of *Pinus sylvestris* and *Quercus robur* (Fig. 5), this relationship, similarly to other species, is described by a quadratic equation. This aligns well with the data obtained through remote sensing methods. The strongest correlations were found between growing stock volume and stand height (see methodology), confirming the feasibility of utilizing remote sensing approaches.

This approach enabled the alignment of ground-based datasets with the spectral sensitivity of Sentinel-1/2 sensors, which capture backscatter and reflectance signals exclusively from the aboveground forest components. Preliminary data analysis shows that using the unsegmented, full dataset yields a very weak correlation ($R^2 = 0.064$).

Comparative statistical analysis confirmed a significant non-linear relationship between forest inventory parameters and modeled aboveground biomass (AGB). The quadratic model proved more accurate than the linear one (the AIC value decreased from 30,718 to 30,682), with the second-order polynomial term being highly significant ($p < 0.001$). Residual analysis (Fig. 6) revealed a characteristic downward curve at high biomass levels (>200 Mg/ha). This indicates a spectral saturation effect in the Sentinel-2 data, which is typical for dense forest canopies.

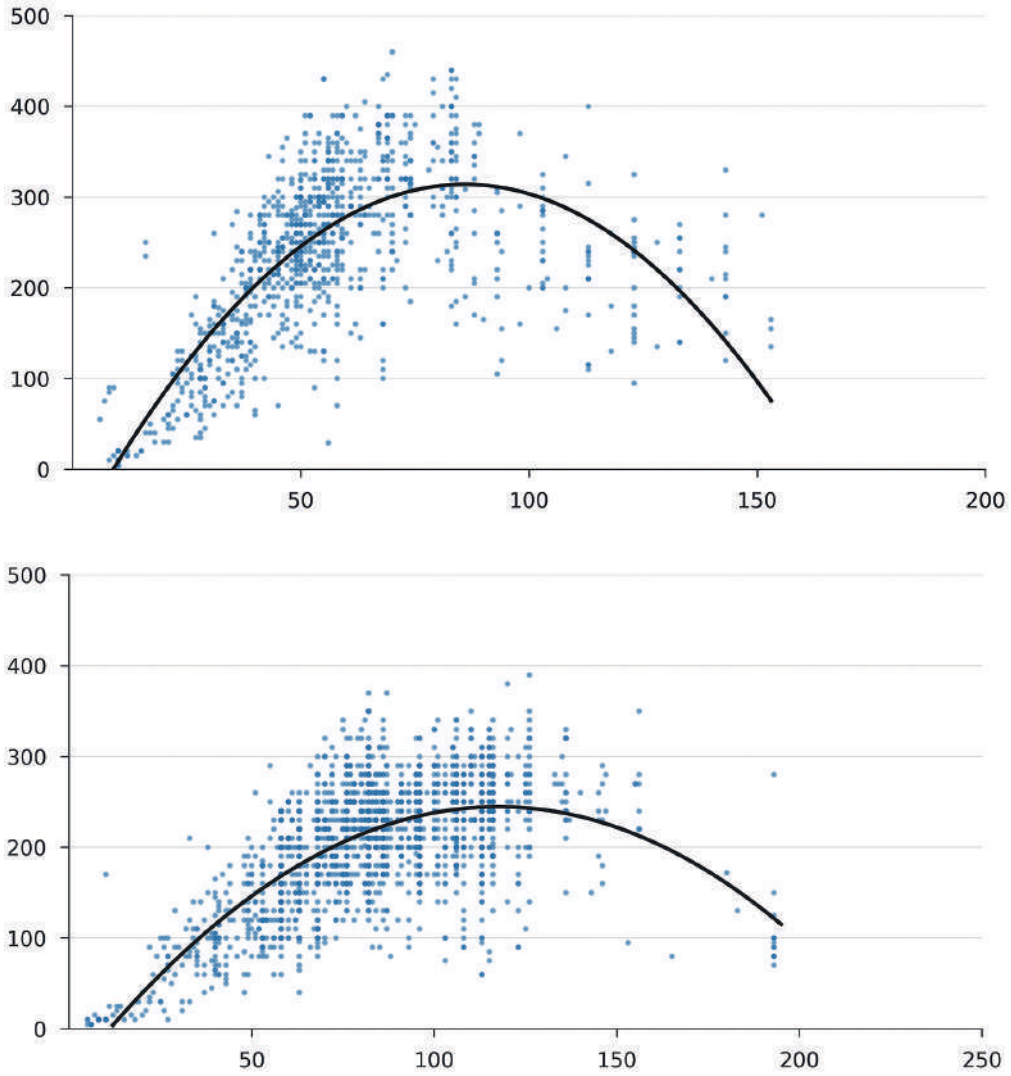


Fig. 5 Dependence of growing stock volume (y) on forest stand age (x) for *Pinus sylvestris*: $y = -0.053x^2 + 9.1089x - 77.376$, $R^2 = 0.53$ (a); *Quercus robur*: $y = -0.0216x^2 + 5.0775x - 53.774$, $R^2 = 0.48$ (b).

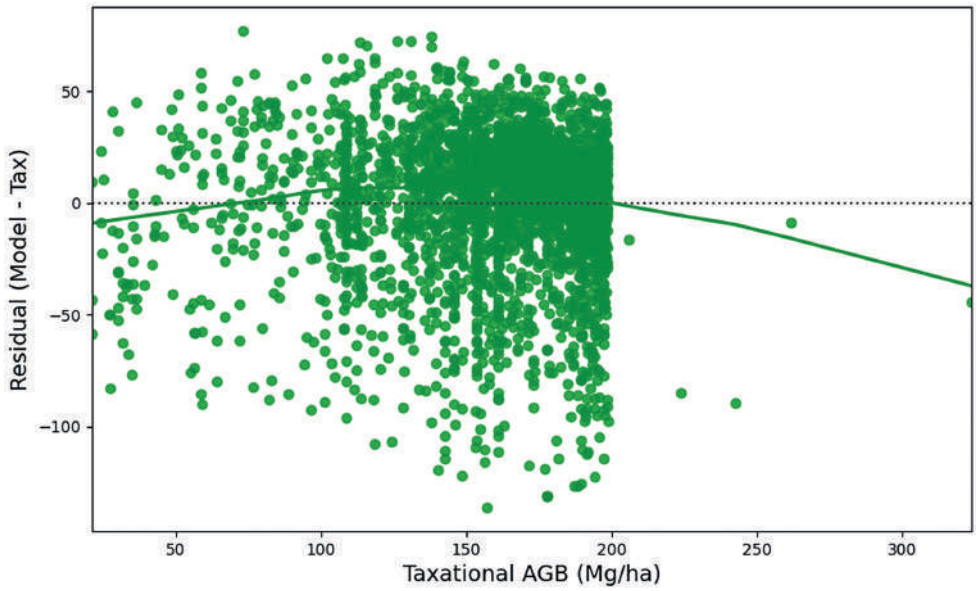


Fig. 6 Residual plot of the linear model.

By comparing the predicted AGB values obtained with the developed Sentinel-1 and Sentinel-2 model against the ground inventory data recalculated for 2022, an initial array of 3,138 validation points was formed. Following the application of the hybrid data filtering algorithm (IQR + MAE threshold), the final dataset for statistical analysis comprised 1,842 points. The analysis showed a substantial improvement in model fit after removing statistical noise. The coefficient of determination (R^2) increased from 0.15 to 0.56, indicating the model's capacity to explain more than half of the biomass variation in the study region. Following the data cleaning process, the mean absolute error (MAE) stabilized at a level below the sample standard deviation, confirming the high representativeness of the model.

A comparative analysis of linear and polynomial regressions on the cleaned data confirmed the assumption of a non-linear relationship. The quadratic model ($y = -0.004195x^2 + 2.1136x - 59.5872$) demonstrated superior statistical performance: a decrease in AIC by 86 units (from 15,636 to 15,550) signifies the greater adequacy of the non-linear approach. The high significance of the quadratic term ($p < 0.001$) mathematically proves the curvature of the regression line.

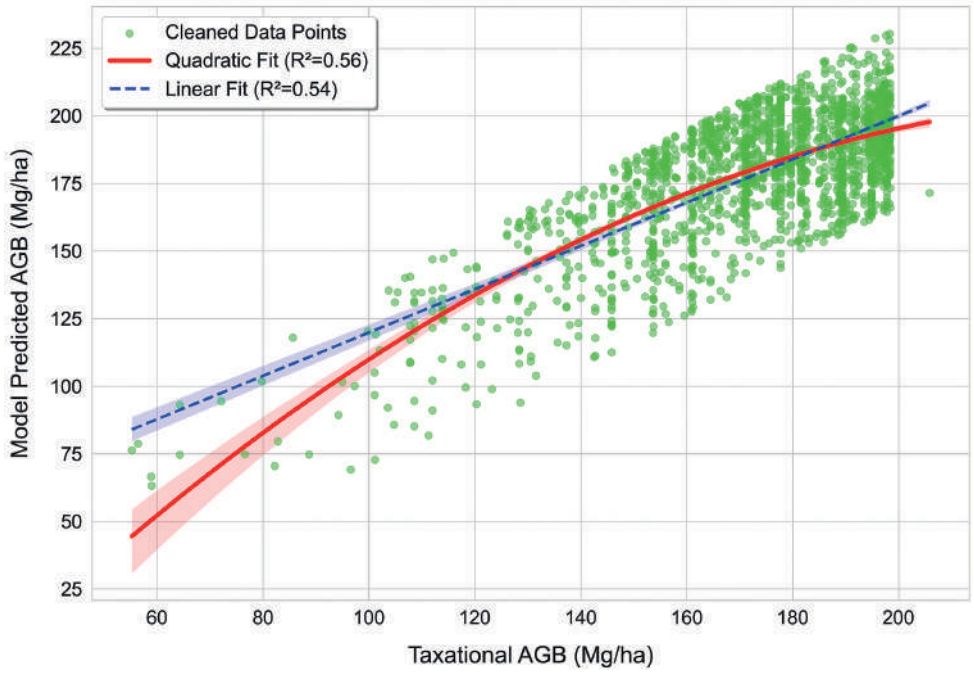


Fig. 7 Scatter plot of taxational vs. predicted AGB with linear and quadratic fit comparison (n = 1,842).

Tab. 3 Statistical indicators of the AGB model approximation for the main forest-forming species.

Species	Number of points (n)	R^2	RMSE (Mg/ha)	Saturation threshold (Mg/ha)
Total sample	1,842	0.564	16.47	251.9
Quercus robur	1,095	0.514	15.33	231.2
Pinus sylvestris s.l.	474	0.545	17.61	278.9
Fraxinus excelsior	166	0.571	17.69	239.7
Alnus glutinosa	63	0.379	16.03	153.3

Visual analysis of the resulting relationship (Fig. 7) indicates a spectral saturation effect. The increase in sensor response gradually slows at biomass values above 180–200 Mg/ha. In such cases, linear approximation leads to a systematic underestimation of stocks in overmature and highly productive stands, whereas the applied quadratic correction partially compensates for this effect.

Calculating the theoretical sensitivity threshold of the model by finding the extremum of the polynomial function revealed a value of 251.9 Mg/ha. This aligns with published literature regarding the signal saturation of the Sentinel-1 C-band radar and Sentinel-2 spectral indices in temperate forests.

Non-linear dynamic analysis of the model showed that the hybrid data cleaning procedure shifted the calculated signal saturation threshold from 198.6 Mg/ha to 251.9 Mg/ha (Tab. 3). This indicates that eliminating random forest inventory errors allowed the model to better identify the weak but existing sensor response in highly productive stands, expanding the reliable biomass prediction range by 27%.

The obtained data indicate a consistently high predictive capacity of the model for most of the studied tree species (Tab. 3). The total model, constructed based on 1,842 test plots, exhibits a coefficient of determination of $R^2 = 0.564$ with a root mean square error (RMSE) of 16.47 Mg/ha. This suggests that the selected calculation methodology adequately replicates the spatial structure of biomass at the landscape level.

Among individual tree species (Tab. 3, Fig. 8), the best approximation results are observed for *Fraxinus excelsior*, where the coefficient of determination reaches 0.571. For the dominant species of the region – *Quercus robur* and *Pinus sylvestris* s.l. – the R^2 values are 0.514 and 0.545, respectively. The somewhat lower indicators for *Alnus glutinosa* ($R^2 = 0.379$) may be associated with a smaller sample size and the specific growing conditions of this species in waterlogged habitats, which affect canopy reflectance.

The saturation threshold parameter warrants particular attention. For *Pinus sylvestris* s.l. it reaches its highest value at 278.9 Mg/ha, which indicates the feasibility of using Sentinel-2 optical data for monitoring mature coniferous stands. Conversely, the lowest saturation threshold was recorded for *Alnus glutinosa* (153.3 Mg/ha), indicating a rapid attainment of maximum canopy density, after which sensor sensitivity to biomass increments decreases substantially.

The obtained RMSE values in the range of 15.33–17.69 Mg/ha across all species are acceptable for remote sensing of forests and confirm the effectiveness of integrating calculated inventory indicators with satellite data to evaluate forest ecosystem services.

To comprehensively evaluate the validity of the obtained results, an analysis of the systematic bias (Bias) of the predicted phytomass values relative to the calculated forest inventory data was performed (Tab. 4).

The obtained results show a minor systematic overestimation (Positive Bias) of the predicted values by the model compared to the calculated ground data. For the entire dataset (n = 1,842) the mean bias is only 5.3 Mg/ha, which corresponds to a relative error of 3.1%. This low indicator confirms the high reliability of the developed algorithm for estimating total biomass stocks. Notably, the highest accuracy was recorded for *Fraxinus excelsior*, where the error is remarkably low at 0.8% (with a bias of 1.36 Mg/ha). This indicates an ideal alignment between the spectral characteristics of this species and the selected mathematical model. For the dominant species, *Quercus robur*, the deviation is also minimal (2.2%), which is a highly significant indicator given that it constitutes the largest sample size in the study (1,095 points). A slightly higher bias is observed for *Pinus sylvestris* s.l. (4.9% or 8.22 Mg/ha), which can be attributed to the structural characteristics of the coniferous canopy and its effect on backscatter and signal scattering in the near-infrared spectrum. The largest relative bias was found in *Alnus glutinosa*

Tab. 4 Comparison of average AGB values and bias indicators for the main tree species.

Name	Number of points (n)	Average (forest inventory)	Average (model)	Bias (Mg/ha)	Error (%)
Total sample	1,842	173.07	178.37	5.3	3.1
Alnus glutinosa	63	152.92	167.88	14.97	9.8
Fraxinus excelsior	166	162.54	163.90	1.36	0.8
Pinus sylvestris s.l.	474	169.28	177.50	8.22	4.9
Quercus robur	1,095	179.04	182.95	3.91	2.2

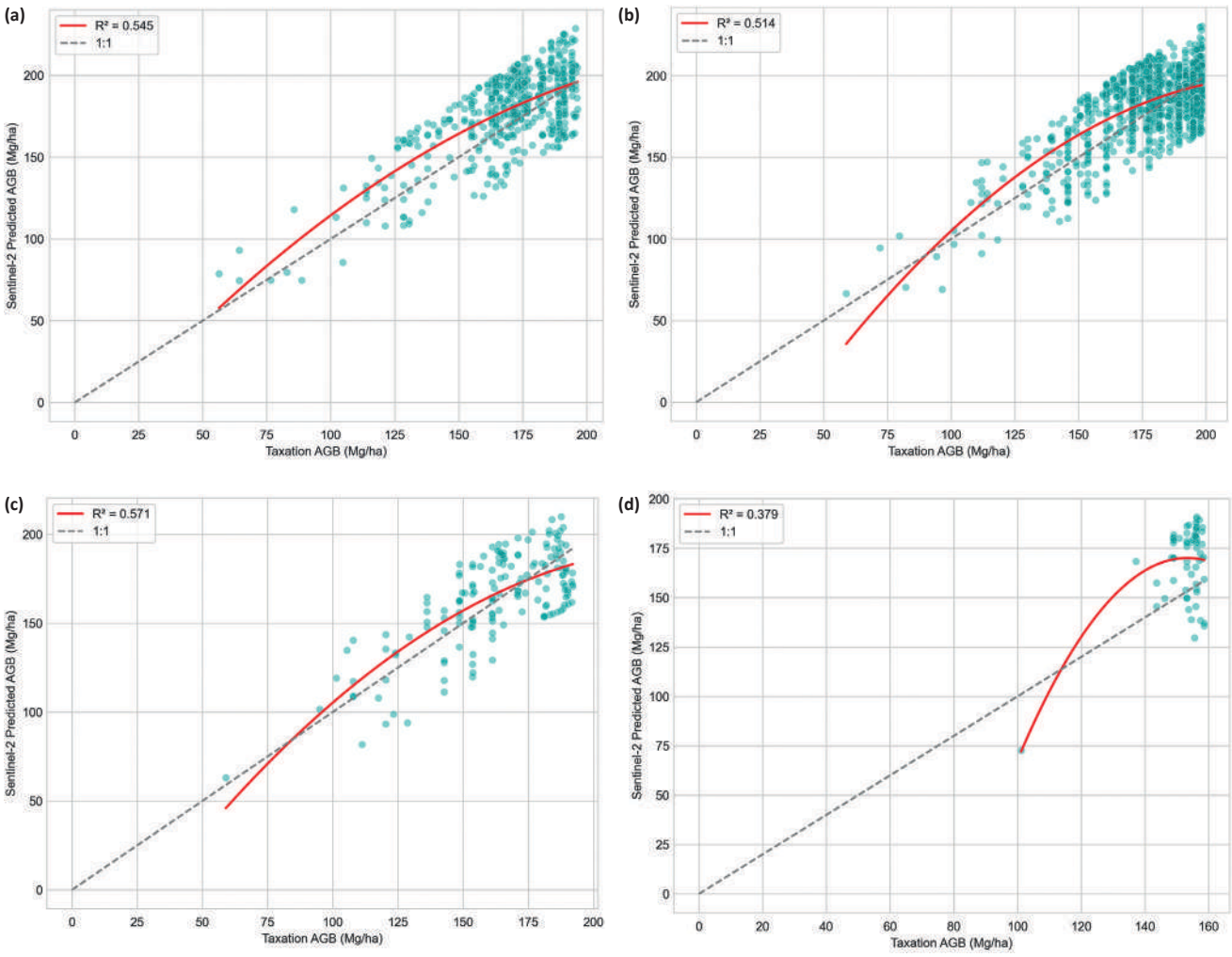


Fig. 8 Validation of AGB estimation models for dominant tree species: *Pinus sylvestris* s.l. (a); *Quercus robur* (b); *Fraxinus excelsior* (c); *Alnus glutinosa* (d).

(9.8%). Although this error is not critical for ecological monitoring in absolute terms (14.97 Mg/ha), it underscores the complexity of biomass modeling in humid locations, where the influence of the underlying surface and soil moisture on the spectral response is most pronounced.

3.4 Validation of the model based on 2014 forest inventory data

To verify the model's resilience to systematic bias caused by natural stand dynamics, we conducted an additional validation based on growing stock volume data from the previous forest inventory of the study area (2014). This approach allowed us not only to verify the accuracy of satellite monitoring but also to justify its applicability for updating outdated national registry data in protected areas, where the last forest inventory was conducted more than 10 years ago.

The total model (Fig. 9), constructed based on a representative sample of 2,454 points (filtered out of an initial 3,138 points), demonstrated a moderate level of consistency ($R^2 = 0.541$) with a root mean square error (RMSE) of 24.4 Mg/ha. The resulting saturation point for the total model is 261.5 Mg/ha. This indicates that while the integrated phytomass indicator for the entire park correctly reflects carbon accumulation trends, it has certain limitations in high-density forest stands, which is typical for optical sensors.

Differentiation of the models by tree species (Tab. 5, Fig. 10) revealed specific features of the satellite signal response depending on canopy structure. *Quercus robur* (n = 1,011) exhibited the highest accuracy among the primary species ($R^2 = 0.598$) with a relatively low error of 20.18 Mg/ha. The model saturation threshold (209.9 Mg/ha) correlates with the biological characteristics of the dense oak canopy structure.

Despite the large sample size, the model for *Pinus sylvestris* (n = 995) demonstrated a slightly lower coefficient of determination ($R^2 = 0.445$). Concurrently, pine displayed the highest saturation threshold at 307.9 Mg/ha, indicating higher model sensitivity to substantial growing stocks specifically within coniferous forest stands. The results for Fraxinus excelsior (n = 192) demonstrated stable accuracy ($R^2 = 0.562$) with an error of 22.81 Mg/ha.

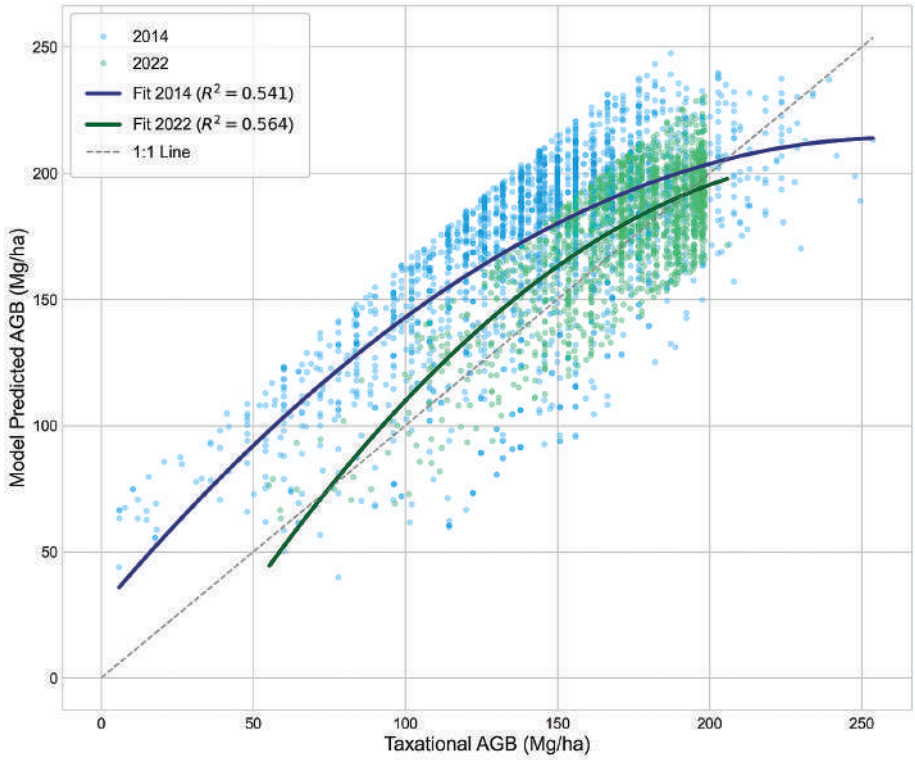


Fig. 9 Relationship between model-predicted AGB for 2022 and taxational (field-observed) validation datasets for 2014 and 2021.

Its saturation threshold (182.1 Mg/ha) is the lowest among the analyzed species, which may suggest a rapid attainment of maximum canopy optical density by this species. The model for *Alnus glutinosa* (n = 99) showed moderate accuracy (R^2 = 0.492) and the lowest absolute error at 18.77 Mg/ha, confirming the feasibility of effective monitoring even within relatively humid habitats.

To gain a deeper understanding of model accuracy, a comparative analysis was conducted between the mean phytomass values derived from forest inventory data and the predicted model values. The results of this analysis for the total sample and key species are presented in Tab. 6.

Analysis of the total sample (n = 2,454) revealed a steady trend toward the overestimation of parameters by the model compared to the forest inventory data. The mean phytomass value predicted by the model is 173.00 Mg/ha, which is 28.52 Mg/ha higher than the inventory-derived value (144.48 Mg/ha). The mean relative error (bias) stands at 19.7%.

Tab. 5 Statistical indicators of the AGB model approximation for the main forest-forming species (based on 2014 forest inventory data).

Group/Species	Number of points (n)	R^2	RMSE (Mg/ha)	Saturation threshold (Mg/ha)
Total sample	2,454	0.541	24.4	261.5
Pinus sylvestris s.l.	995	0.445	27.53	307.9
Quercus robur	1,011	0.598	20.18	209.9
Fraxinus excelsior	192	0.562	22.81	182.1
Alnus glutinosa	99	0.492	18.77	190

The degree of data consistency varies substantially depending on the biological characteristics of the tree species. *Pinus sylvestris* s.l. and *Alnus glutinosa* demonstrated the lowest levels of relative bias – 16.6% and 16.5%, respectively. This indicates a high stability of the model for these stand types, where the error remains within the range of natural annual increment and the typical margins of error of standard forest inventory methods. The largest bias was recorded for *Quercus robur* (23.5%) and *Fraxinus excelsior* (19.9%). The high deviation level for oak (an absolute bias of 32.99 Mg/ha) may be associated with an underestimation of actual growing stocks in older forest inventory records, given that the broadleaved hardwood forests of the park are characterized by a high proportion of associated understory layers and significant biomass accumulation. Consequently, the detected bias does not represent an algorithmic error but rather reflects the dynamic changes within the park's ecosystems that occurred after the last forest inventory.

When comparing the overall validation scatter plot (Fig. 9) with the plots for individual species (Fig. 10), a specific discrepancy in the behavior of the regression curves relative to the 1:1 line of perfect agreement was identified. On the individual species plots (*Quercus robur*, *Pinus sylvestris* s.l., *Fraxinus excelsior*, *Alnus glutinosa*), the regression curves are positioned

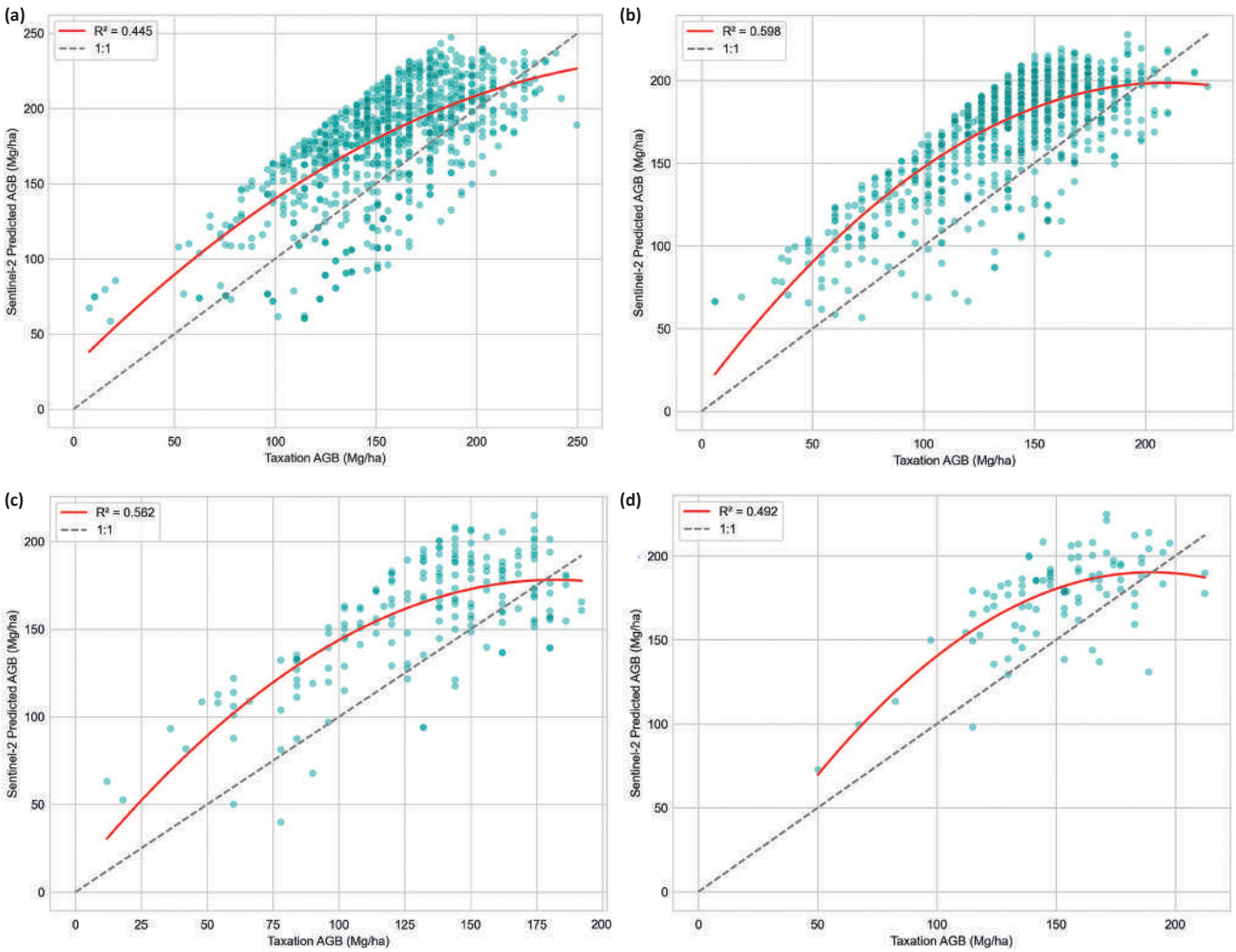


Fig. 10 Validation of AGB estimation models for dominant tree species (based on 2014 forest inventory data): *Pinus sylvestris* s.l. (a); *Quercus robur* (b); *Fraxinus excelsior* (c); *Alnus glutinosa* (d).

almost entirely above the 1:1 line. This confirms the presence of a systematic positive bias driven by biological factors: the actual phytomass increment since the last forest management assessment and the understory contribution, which is captured by satellite sensors but omitted in standard forest inventories. In this scenario, the model adapts to the specific point cloud of a given species, describing its internal structure with maximum precision.

In contrast, the overall validation plot presents a different scenario: a significant portion of the curve (particularly at extreme values) tends toward or falls below the 1:1 line. This effect – which is also observed on the validation plots based on the 2022 calculated biomass, albeit less pronounced (Fig. 8–9) – is attributed to statistical averaging and the saturation effect. When combining different tree species into a single dataset, the model encounters a high variability in spectral response. To minimize the overall mean square error (MSE), the regression algorithm is forced to select a more conservative trajectory that passes through the geometric center of the combined point cloud. When biomass accumulation exceeds 200 Mg/ha, the spectral sensitivity of the satellite bands decreases substantially. Since the number of such high-value points in the total sample is limited, this

Tab. 6 Comparison of average AGB values and bias indicators for the main tree species.

Name	Number of points (n)	Average (Forest inventory)	Average (Model)	Bias (Mg/ha)	Error (%)
Total sample	2,454	144.48	173.00	28.52	19.7
Pinus sylvestris s.l.	995	154.57	180.21	25.64	16.6
Quercus robur	1,011	140.35	173.35	32.99	23.5
Fraxinus excelsior	192	132.14	158.46	26.32	19.9
Alnus glutinosa	99	151.53	176.46	24.93	16.5

leads to an underestimation of predictions for highly productive plots.

Consequently, the comparative analysis of the two verification methods enabled the differentiation between the technical accuracy of the model and the biological dynamics of the target object. The application of the calculated approach (with verification based on biomass calculated from morphometric parameters) demonstrated the high accuracy of the developed model (R^2 = 0.56), where the regression line closely approximated the 1:1 isoline (Fig. 10). This proves that when the temporal lag is correctly accounted for, Sentinel-1/2 satellite data provide precise estimations of aboveground phytomass. At the same time, verification based on growing stock volume data revealed a consistent positive bias. Considering the outcomes of the first approach, this bias should be interpreted not as a systematic modeling error, but rather as a reflection of the actual accumulated biomass increment and the contribution of ecosystem components that were omitted from standard forest inventory descriptions.

3.5 Estimation of aboveground biomass stocks in key forest habitats of the "Svyati Hory" National Nature Park and its losses over the 2022–2024 period

Based on forest inventory data and the results of satellite image analysis, we have developed a habitat classification scheme and created a corresponding map that adequately represents their diversity (Fig. 11).

To estimate the aboveground biomass stocks across the primary forest habitats of the Park (Fig. 11), model calibration was performed. The calibration process of the predictive model was based on approximating the relationship between the predicted aboveground biomass values and the verified ground-based forest inventory data (n = 1,842).

Comparative analysis of statistical criteria confirmed the superiority of the quadratic model (R^2 = 0.5645; AIC = 15,550.48) over the linear one due to its more precise description of the non-linear relationship in the high phytomass range. The resulting calibration equation, AGB = $-0.004195x^2 + 2.1136x - 59.5872$, minimized the root mean square error to RMSE = 16.47 Mg/ha. The negative coefficient of the quadratic term mathematically verifies the gradual saturation effect of the remote sensing signal; however, the synergy between the optical SWIR bands and Sentinel-1 radar data ensures model stability even upon reaching threshold biomass values (exceeding 200 Mg/ha), which is confirmed by the low internal variability of the predictions (CV < 10%).

The results of the zonal statistics (Tab. 7) indicate significant spatial and structural heterogeneity of aboveground biomass stocks within the studied habitats. The total area of forest ecosystems was 37,097.24 ha, and the cumulative aboveground phytomass stock is estimated at 14.22 million tonnes. The

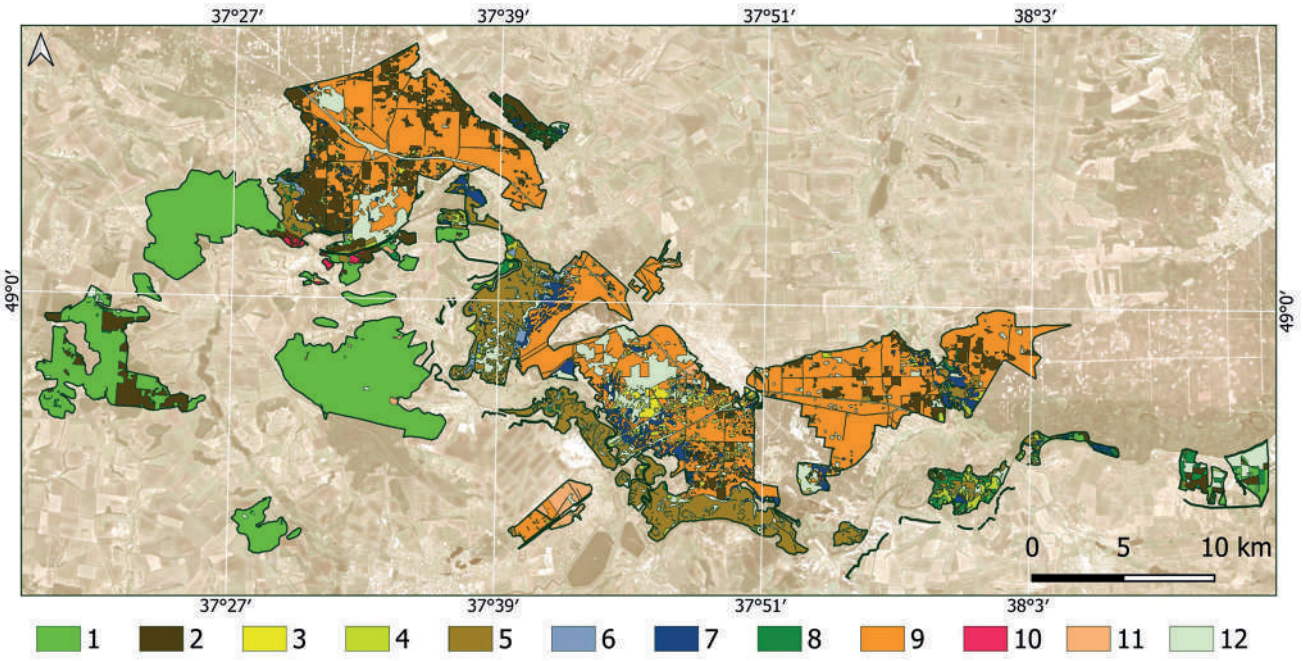


Fig. 11 Forest vegetation habitats of the "Svyati Hory" National Nature Park: 1 – *Carpinus* and *Quercus* mesic deciduous forest (T1E); 2 – Thermophilous or Acidophilous oak-dominated forest (T199, T1B); 3 – Temperate and boreal mountain *Betula* and *Populus tremula* forest on mineral soils (T1C); 4 – Temperate *Salix* and *Populus* riparian forest (T11); 5 – Sarmatic riverine oak forests (T1315); 6 – Sarmatic ash-alder forests (T12135); 7 – Ponto-Pannonic tall herb ash-alder forests (T12133); 8 – Broadleaved deciduous plantation of non-native trees (T1H); 9 – Temperate continental *Pinus sylvestris* forest (G3.4232 Sarmatic steppes *Pinus sylvestris* forests) (T35); 10 – Temperate continental *Pinus sylvestris* forest (G 3.4G *Pinus sylvestris* on chalk in the steppe zone) (T35); 11 – Coniferous plantation (T3N, T3M); 12 – Other habitats. Topobase – Google Satellite.

Tab. 7 Phytomass indicators of the dominant habitat types in the "Svyati Hory" National Nature Park (as of 2022). For full names of habitats see Fig. 11.

No	Habitats codes	Area (ha)	ABGB (Mg)	Area (ha) (burned)	ABGB (Mg) (burned)	Area (%) (burned)	ABGB (%) (burned)
1	T3N, T3M	505.75	180,394.47	157.06	57,455.27	31.05	31.85
2	T35 (G3.4232)	13,903.20	5,215,690.24	9,029.91	3,556,351.33	64.95	68.19
3	T35 (G3.4G)	96.30	32,679.11	35.25	14,189.67	36.60	43.42
4	T12135	282.21	110,513.85	29.47	7,148.72	10.44	6.47
5	T1E	9,355.97	3,906,041.68	79.80	23,542.40	0.85	0.60
6	T199, T1B	4,767.93	1,893,299.87	1,810.56	758,538.33	37.97	40.06
7	T12133	1,641.03	570,330.42	338.86	111,376.80	20.65	19.53
8	T1C	752.47	222,873.64	330.70	97,613.19	43.95	43.80
9	T11	661.06	220,107.56	36.01	8,917.43	5.45	4.05
10	T1315	4,338.87	1,649,253.49	52.28	16,418.96	1.20	1.00
11	T1H	792.44	216,785.96	60.54	12,704.05	7.64	5.86
	Total	37,097.24	14,217,970.28	11,960.43	4,664,256.15		

maximum specific biomass values are characteristic of *Carpinus* and *Quercus* mesic deciduous forest (T1E) at 180.06 Mg/ha. This confirms the high productivity of the region's climax oak forests. High values are also exhibited by Thermophilous and Acidophilous oak-dominated forests on terraces (171.01 Mg/ha). The primary carbon sinks are Temperate continental *Pinus sylvestris* forest / Sarmatic steppes *Pinus sylvestris* forests (T35/G3.4232), accounting for over 5.2 million tonnes of phytomass. Despite their slightly lower density (161.60 Mg/ha) compared to oak forests, they dominate the total balance due to having the largest distribution area (13,903 ha). Sarmatic ash-alder forests (T12135), although covering a small area (282 ha), exhibit a high phytomass density of 168.72 Mg/ha, indicating their significant energy potential in humid locations. The lowest biomass density was recorded in Broadleaved deciduous plantation of non-native trees (T1H) at 118.04 Mg/ha, which is primarily explained by the shrub-like structure or young age of the plantations (apricot, smoketree, honey locust, etc.).

Zonal analysis of phytomass distribution confirmed that over 64% of the total AGB stocks are concentrated in two habitat types: Temperate continental *Pinus sylvestris* forest (G3.4232 Sarmatic steppes *Pinus sylvestris* forests) and *Carpinus* and *Quercus* mesic deciduous forest. The obtained data serve as a baseline for the subsequent evaluation of ecosystem service losses resulting from pyrogenic impacts and mechanical damage to the stands.

Following the outbreak of the armed conflict in 2022 in the vicinity of the Park, the frequency of forest fires within its forested areas increased sharply.

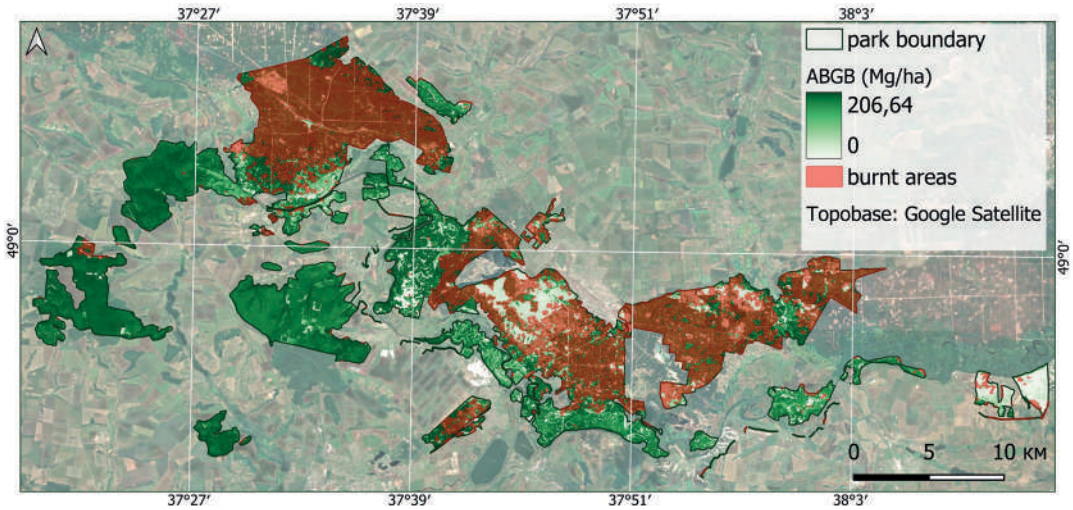


Fig. 12 Cartographic model of aboveground biomass density and areas burned during the 2022–2024 period within the "Svyati Hory" National Nature Park.

Consequently, substantial territories of the Park sustained pyrogenic damage, which is clearly identifiable on satellite imagery. Based on the visual interpretation and comparative analysis of Sentinel-2 satellite images (2021–2024), these affected areas (burn scars) were delineated, and a GIS layer outlining the boundaries of the burned forests (burn scar mask) was subsequently generated (Fig. 12).

To quantitatively evaluate the destructive impact of fire on the forest ecosystems, a spatial overlay analysis was applied. The burn scar mask layer, derived from satellite imagery interpretation, was superimposed onto the habitat map. This allowed for the isolation of habitat fragments that directly sustained pyrogenic impacts and enabled a secondary zonal statistics analysis to be conducted for these specific areas (Tab. 7).

The total area of forest stands affected by fire is 11,960.43 ha. The cumulative losses of aboveground phytomass within the fire mask boundaries are estimated at 4,664,256.15 tonnes. The most destructive impact was recorded in Temperate continental *Pinus sylvestris* forest / Sarmatic steppes *Pinus sylvestris* forests (T35/G3.4232). Fires engulfed 64.95% of the total area of this habitat (9,029.91 ha), resulting in the loss of 3.56 million tonnes of AGB, which constitutes 68.19% of the entire stock of this forest type within the park. Significant losses were also sustained by birch forests (43.95% of their area) and oak-pine forests on terraces (37.97% of their area). For the latter, the volume of lost biomass exceeded 758 thousand tonnes. The lowest relative impact was recorded for *Carpinus* and *Quercus* mesic deciduous forest (T1E) and Sarmatic riverine oak forests (T1315), where the area of burn scars did not exceed 0.85–1.2%.

Particular attention should be paid to the status of Temperate continental *Pinus sylvestris* forest / *Pinus sylvestris* on chalk in the steppe zone (T35/G 3.4G), which represents a unique regional ecosystem based on the chalk pine (*Pinus sylvestris* var. *cretacea*). According to the results of the overlay analysis, 36.6% of the area of this rare habitat fell within the burned territories, resulting in the loss of 14.19 thousand tonnes of aboveground biomass (Table 7). Notably, certain patches of this habitat were completely destroyed by fire, while the majority of the remaining areas sustained severe damage.

4. Discussion

Spatial resolution is critical for forest biomass modeling. Our findings demonstrate that 10 m resolution (R^2 = 0.575) significantly outperforms 30 m resolution (R^2 = 0.281) by reducing the pixel-averaging effect. In fragmented mosaic landscapes, the 30 m resolution causes artificial smoothing of spectral responses, underestimating maximum and overestimating minimum biomass values (Duncanson et al. 2022; Lang et al. 2023). Conversely, 10 m data better represent canopy fine structure and delineate forest infrastructure (Phiri et al. 2020; Lang et al. 2023).

Predictor-importance analysis indicates that optical indices based on the visible spectrum, such as NDVI, lose explanatory power in highly productive forests. The strong contributions of the SWIR band (B12) and DEM reflect their ability to capture canopy structure and moisture, as SWIR bands penetrate deeper into the canopy and delay spectral saturation (Zhao et al. 2016). Additionally, the NDRE index performance confirms that the red-edge region is a more reliable biomass indicator in dense stands than broadband channels (Pandit et al. 2018). Integrating optical data with Sentinel-1 radar metrics (VV, VH) enhances model sensitivity to vertical stem structure, supporting a robust multisensor approach.

A key contribution of this study is mitigating the spectral saturation effect, which typically limits optical data use at 150–200 Mg/ha (Hao and Huang 2023). Implementing quadratic regression and a two-stage hybrid filtering algorithm (IQR + MAE) shifted the sensitivity threshold from 198.6 to 251.9 Mg/ha. This enabled accurate growing stock estimation in overmature *Pinus sylvestris* stands and climax *Quercus robur* forests, where linear models systematically underestimate biomass. The small positive model bias (+3.1%) relative to forest inventory data is biologically plausible, as satellite sensors capture integrated phytomass (understory and herb layers) and recent wood increment, which are frequently omitted from historical management records.

Since the outbreak of the armed conflict in 2022, the forest ecosystems of "Svyati Hory" National Nature Park have sustained catastrophic damage, losing an estimated 4.66 million tonnes of above-ground biomass across 11.9 thousand hectares. This substantial loss of growing stock releases stored carbon into the atmosphere, transforming the area from a carbon sink into a carbon source (Matsala et al. 2024). Spatial overlay analysis revealed distinct pyrogenic vulnerability across habitat types. Boreal complexes, specifically sarmatic steppe pine forests (G3.4232), suffered the most destructive impact, losing 68.19% of their biomass. The high vulnerability of *Pinus sylvestris* is driven by flammable essential oils, dry coniferous litter accumulation, a canopy structure promoting crown fires, and its location on dry sandy terraces (Bowman et al. 2009). Conversely, mesophilic and hygrophilous broadleaved forests (habitats T1E, T1315) with *Quercus robur*, *Fraxinus excelsior*, and *Alnus glutinosa* demonstrated high resilience, with biomass losses below 1–2%. High foliage moisture, lack of flammable understory, and humid floodplain positioning allowed these habitats to act as natural fire barriers, underscoring the importance of mosaic landscape structures for pyrogenic resilience.

The *Pinus sylvestris* on chalk (G3.4G) habitat requires critical conservation focus; it lost 36.6% of

its area and 14.19 thousand tonnes of biomass, threatening a community of European significance (Ministry of Environmental Protection and Natural Resources of Ukraine 2021; Council of Europe 2018). Chalk pine (*Pinus sylvestris var. cretacea*) is a narrow-range endemic and Tertiary relict. Due to specific edaphic conditions and low early-stage competitive ability, natural post-fire regeneration may take decades or prove impossible without human intervention. The absence of serotinous cones means crown fires destroy the seed bank, while the thin litter layer on chalk breaks down too quickly for seedlings to establish, making artificial reforestation the only viable restoration pathway (Fernandes et al. 2008; Matsala et al. 2024).

Despite high model accuracy (R^2 = 0.564), certain limitations remain. Utilizing 2014 forest inventory records introduces temporal mismatch risks. Although mitigated via mathematical modeling of forest increment and hybrid filtering, synchronous field data remain ideal. This model estimates aboveground biomass exclusively; substantial carbon was also lost through litter burning and topsoil degradation, requiring further investigation. Future research should focus on satellite time-series monitoring of post-fire regeneration and quantifying ecosystem service economic losses.

5. Conclusions

For monitoring fragmented forest landscapes, a 10 m spatial resolution is optimal. Transitioning from 30 m to 10 m data increased model accuracy (R^2 from 0.28 to 0.58) and mitigated the pixel-averaging effect, enhancing the detection of low-biomass and highly fragmented tracts.

The SWIR bands and DEM had the strongest influence on model performance, highlighting the importance of canopy moisture and geomorphology, while the incorporation of the NDRE index and Sentinel-1 radar metrics helped mitigate spectral saturation in dense stands.

Implementing a quadratic regression model extended the reliable biomass prediction range to 251.9 Mg/ha, representing a 27% increase over the linear alternatives. The observed positive model bias (+3.1%) can be attributed to the inclusion of understory phytomass and recent wood increment rather than to systematic error.

The 2022–2024 conflict sparked widespread fires, destroying 32.8% of the park's total above-ground biomass. Among these, coniferous ecosystems proved the most vulnerable, with steppe pine forests losing over 3.5 million tonnes of biomass.

Endemic chalk pine forests (*Pinus sylvestris var. cretacea*) face critical degradation, having lost nearly 40% of their area. Combined with soil erosion and seed bank destruction, natural post-fire recovery is severely hindered, necessitating targeted artificial reforestation strategies following comprehensive humanitarian demining.

To establish a baseline for a long-term research agenda, future studies should focus on monitoring post-conflict vegetation succession across the affected areas over the coming decades. Understanding recovery trajectories is particularly critical for vulnerable habitats such as endemic chalk pine ecosystems, where natural regeneration may take decades or require active restoration interventions. The multisensor remote sensing framework developed in this study can be transformed into a continuous long-term observatory to track ecosystem dynamics and biomass accumulation over time. However, widespread contamination by unexploded ordnance and landmines presents a severe operational constraint, limiting ground-based safety, delaying active restoration efforts, and restricting field validation protocols. Incorporating safe, non-invasive remote sensing techniques will therefore remain paramount for assessing post-war ecological recovery in hazardous landscapes.

Acknowledgments

This work was carried out within the target program of the National Academy of Sciences of Ukraine 'Support for the Development of Priority Research Areas' under the project 'Development and application of methodology and algorithms for assessing the impact of military operations on the phytodiversity of natural ecosystems in Ukraine to determine their losses, recovery, and adaptive potential' with the support of the NGO 'Environment People Law' (EPL).

References

Al-Saady, Y., Merkel, B., Al-Tawash, B., Al-Suhail, Q. (2015): Land use and land cover (LULC) mapping and change detection in the Little Zab River Basin (LZRB), Kurdistan Region, NE Iraq and NW Iran. FOG – Freiberg Online Geoscience 43, 1–32.

Bowman, D. M., Balch, J. K., Artaxo, P., Bond, W. J. (2009): Fire in the Earth system. Science 324(5926), 481–484, https://doi.org/10.1126/science.1163886.

Didukh, Y. P., Pashkevych, N. A. (2003): Ecological patterns of vegetation distribution in the "Sviati Hory" National Nature Park. Ukrainian Phytosociological Collection 1(20), 83–98.

Didukh, Ya. P., Sokolenko, U. M., Rasevych, V. V., Havrylov, S. O. (2024): Methodology for calculating environmental damage to natural ecosystems and their components: A manual. Kravchenko, O. V. (Ed.); Manuscript Company Publishing House: Lviv – Kyiv, Ukraine, 68 p. (in Ukrainian).

Doronin, Yu. A. (1970): Current state of chalk pine forests of the Central Russian Upland. Izvestiya Voronezhskogo

gosudarstvennogo pedagogicheskogo instituta 112, 28–35 (in Russian).

Dubayah, R., Armston, J., Healey, S. P., Yang, Z., Patterson, P. L., Saarela, S., Stahl, G., Duncanson, L., Hancock, S. (2022): GEDI launches a new era of biomass inference from space. Environmental Research Letters 17(9): 095001, https://doi.org/10.1088/1748-9326/ac8694.

Duncanson, L., Kellner, J., Armston, J., Dubayah, R. (2022): Aboveground biomass density models for NASA's Global Ecosystem Dynamics Investigation (GEDI) lidar mission. Remote Sensing of Environment 270: 112845, https://doi.org/10.1016/j.rse.2021.112845.

Dyakova, O. V. (2008): Vegetation of alder forests in the Svyatohirskyi Tabir tract (Svyati Hory National Nature Park). In Hlukhov, O. Z. (Ed.), Restoration of Damaged Natural Ecosystems: Materials of the Third International Scientific Conference; Donetsk, Ukraine, pp. 183–185 (in Ukrainian).

EUNIS – European Nature Information System. Available online: https://eunis.eea.europa.eu/ (accessed on 18 May 2026).

Fayad, I., Ciais, P., Schwartz, M., Wigneron, J. P., Baghdadi, N., de Truchis, A., d'Aspremont, A., Frappart, F., Saatchi, S., Sean, E., Pellissier-Tanon, A., Bazzi, H. (2024): Hy-TeC: a hybrid vision transformer model for high-resolution and large-scale mapping of canopy height. Remote Sensing of Environment 302: 113945, https://doi.org/10.1016/j.rse.2023.113945.

Fernandes, P. M., Vega, J. A., Jiménez, E., Rigolot, E. (2008): Fire resistance of European pines. Forest Ecology and Management 256(3), 246–255, https://doi.org/10.1016/j.foreco.2008.04.032.

Gorelick, N., Hancher, M., Dixon, M., Ilyushchenko, S., Thau, D., Moore, R. (2017): Google Earth Engine: Planetary-scale geospatial analysis for everyone. Remote Sensing of Environment 202, 18–27, https://doi.org/10.1016/j.rse.2017.06.031.

Grings, F., Leszczuk, A., Hildt, E., Lorán, D., Arellana, J., Orona, M., Lopez, H., Kornuta, J., Ottenweller, C., Breziski, D., Silva, H., Rechberger, F., Franco, M. (2025): Validation of GEDI above ground biomass product over Pinus sp. plantations in Argentina. Journal of Applied Remote Sensing 19(2): 024502, https://doi.org/10.1117/1.JRS.19.024502.

Groshev, B. I., Sinitsyn, S. G., Moroz, P. I., Seperovich, I. P. (1980): Forest Inventory Handbook, 2nd ed.; Lesnaya promyshlennost: Moscow, USSR, 287 p. (in Russian).

Hao, Q., Huang, C. (2023): A review of forest aboveground biomass estimation based on remote sensing data. Chinese Journal of Plant Ecology 47(10), 1356–1374, https://doi.org/10.17521/cjpe.2023.0008.

Harris, N. L., Gibbs, D. A., Baccini, A., Birdsey, R. A., de Bruin, S., Farina, M., Fatoyinbo, L., Hansen, M. C., Herold, M., Houghton, R. A., Potapov, P. V., Suarez, D. R., Roman-Cuesta, R. M., Saatchi, S. S., Slay, C. M., Turubanova, S. A., Tyukavina, A. (2021): Global maps of twenty-first century forest carbon fluxes. Nature Climate Change 11(3), 234–240, https://doi.org/10.1038/s41558-020-00976-6.

Hylyarov, A. M. (1967): Information theory in ecology. Uspekhi sovremennoy biologii 64(4), 107–115 (in Russian).

Kotov, M. I. (1928): "Svyati Hory" of the Artemivsk district. Materialy po okhrane prirody Ukrainy 1, 115–126 (in Russian).

Lakida, P. I. (2002): Forest Phytomass of Ukraine; Zbruch: Ternopil, Ukraine, 256 p. (in Ukrainian).

Lang, N., Jetz, W., Schindler, K., Wegner, J. D. (2023): A high-resolution canopy height model of the Earth. Nature Ecology & Evolution 7(11), 1778–1789, https://doi.org/10.1038/s41559-023-02206-6.

Liang, M., González-Roglich, M., Roehrdanz, P., Tabor, K., Zvoleff, A., Leitold, V., Silva, J., Fatoyinbo, L., Hansen, M., Duncanson, L. (2023): Assessing protected area's carbon stocks and ecological structure at regional-scale using GEDI lidar. Global Environmental Change 78: 102621, https://doi.org/10.1016/j.gloenvcha.2022.102621.

Matsala, M., Odruzhenko, A., Hinchuk, T., Myroniuk, V., Drobyshev, I., Sydorenko, S., Zibtsev, S., Milakovsky, B., Schepaschenko, D., Kraxner, F., Bilous, A. (2024): War drives forest fire risks and highlights the need for more ecologically-sound forest management in post-war Ukraine. Scientific Reports 14: 4131, https://doi.org/10.1038/s41598-024-54811-5.

Ministry of Environmental Protection and Natural Resources of Ukraine (2021): Order No. 111 "On approval of lists of plant and fungal species included in the Red Data Book of Ukraine (flora), and plant and fungal species excluded from the Red Data Book of Ukraine (flora)". Available online: https://zakon.rada.gov.ua/laws/show/z0370-21#n17 (accessed on 18 May 2026) (in Ukrainian).

Kuzemko, A. A., Didukh, Ya. P., Onyshchenko, V. A., Sheffer, Ya. (Eds.) (2018): National Habitat Catalogue of Ukraine; Klymenko Yu. Ya.: Kyiv, Ukraine, 442 p. (in Ukrainian).

Pandit, S., Tsuyuki, S., Dube, T. (2018): Estimating above-ground biomass in sub-tropical buffer zone community forests, Nepal, using Sentinel 2 data. Remote Sensing 10(4): 601, https://doi.org/10.3390/rs10040601.

Pauls, J., Zimmer, M., Kelly, U. M., Schwartz, M., Saatchi, S., Ciais, P., Pokutta, S., Brandt, M., Gieseke, F. (2024): Estimating canopy height at scale, arXiv:2406.01076, https://doi.org/10.48550/arXiv.2406.01076.

Pereira, P., Bašić, F., Bogunovic, I., Barceló, D. (2022): Russian-Ukrainian war impacts the total environment. Science of the Total Environment 837: 155865, https://doi.org/10.1016/j.scitotenv.2022.155865.

Phiri, D., Simwanda, M., Salekin, S., Nyirenda, V. R., Murayama, Y., Ranagalage, M. (2020): Sentinel-2 data for land cover/use mapping: a review. Remote Sensing 12(14): 2291, https://doi.org/10.3390/rs12142291.

Potapov, P., Li, X., Hernandez-Serna, A., Tyukavina, A., Hansen, M. C., Kommareddy, A., Pickens, A., Turubanova, S., Tang, H., Silva, C. E., Armston, J., Dubayah, R., Blair, J. B., Hofton, M. (2021): Mapping global forest canopy height through integration of GEDI and Landsat data. Remote Sensing of Environment 253: 112165, https://doi.org/10.1016/j.rse.2020.112165.

Council of Europe (2018): Revised Annex I to Resolution 4 (1996) of the Bern Convention on endangered natural habitat types using the EUNIS habitat classification. Adopted by the Standing Committee on 30 November 2018. Available online: https://rm.coe.int/16807469e7 (accessed on 18 May 2026).

Sedano, F., Maianti, P., Boca, R., Suarez-Moreno, M., Broglia, M. et al. (2026): Advance report on Forest Fires in

Europe, Middle East and North Africa 2025; Publications Office of the European Union: Luxembourg, https://doi.org/10.2760/3859043.
Shao, Z., Zhang, L. (2016): Estimating forest aboveground biomass by combining optical and SAR data: A case study in Genhe, Inner Mongolia, China. Sensors 16(6): 834, https://doi.org/10.3390/s16060834.
Sinelshchikov, R. G. (1975): Common hornbeam in the forests of Donbas. Vvedenie v eksperimentalnuyu ekologiyu rasteniy 4, 24–29 (in Russian).
Tassi, A., Vizzari, M. (2020): Object-oriented LULC classification in Google Earth Engine combining SNIC, GLCM, and machine learning algorithms. Remote Sensing 12(22): 3776, https://doi.org/10.3390/rs12223776.
Tolan, J., Yang, H. I., Nosarzewski, B., Couairon, G., Vo, H. V., Brandt, J., Couprie, C. (2024): Very high resolution canopy height maps from RGB imagery using self-supervised vision transformer and convolutional decoder trained on aerial lidar. Remote Sensing of Environment 300: 113888, https://doi.org/10.1016/j.rse.2023.113888.
Van Winckel, S., Simons, J., Lhermitte, S., Muys, B. (2025): Assessing the effect of forest management on above-ground carbon stock by remote sensing. Biogeosciences 22, 4291–4307, https://doi.org/10.5194/bg-22-4291-2025.
Zhurova, P. T. (2012): National Nature Park "Svyati Hory". In Ecology and Natural Resources of Ukraine; Ukrainian Union of Journalists, Instytut biohrafichnykh doslidzhen: Kyiv, Ukraine, 79 p. (in Ukrainian).
Zibtsev, S., Pasternak, V., Vasylyshyn, R., Sydorenko, S., Soshenskyi, O., Myroniuk, V. (2024): Assessment of carbon emissions due to landscape fires in Ukraine during war in 2022. Ukrainian Journal of Forest and Wood Science 15(1), 126–139, https://doi.org/10.31548/forest/1.2024.126.